## Title

Effect of structure-to-foundation mass ratio in analytical modeling of soil-foundation-structure interaction during earthquakes



## Authors

Ko, Kil-Wan
Kayen, Robert E

## Publication Date

2023-09-01

## DOI

10.1016/j.soildyn.2023.108050

Peer reviewed

Soil Dynamics and Earthquake Engineering 172 (2023) 108050

Contents lists available at ScienceDirect

Soil Dynamics and Earthquake Engineering

journal homepage: www.elsevier.com/locate/soildyn

# Effect of structure-to-foundation mass ratio in analytical modeling of soil-foundation-structure interaction during earthquakes

Kil-Wan Ko, Robert E. Kayen *

*Dept. of Civil and Environmental Eng., University of California, Berkeley, CA, USA*

ARTICLE INFO

*Keywords:*
Structure-to-foundation mass ratio
Soil–foundation–structure interaction
Analytical modeling
Stockwell transform
Shallow foundation

ABSTRACT

The vertical factor of safety ($FS_v$) of shallow foundations has been widely used for static design and seismic design. The $FS_v$ is a function of the bearing capacity of the system and the vertically applied load from the structure and foundation loads to the soil and foundation interface. However, the structure-to-foundation mass ratio ($MR$) can be different for the systems presenting the same $FS_v$. The dynamic responses of the structure and foundation system depend on the $MR$ as it develops dissimilar inertial behaviors from the structure and foundation. In this study, the effect of $MR$ on the structure and foundation responses was evaluated using an analytical model that enables influence of the nonlinearity of the soil on the modeled foundation base and structure. For systems with the same $FS_v$ under identical input loading conditions, the inertial behavior of heavy foundations had a larger acceleration response than the lighter foundations. Consequently, $MR$ should be considered for evaluating dynamic soil-foundation-structure interaction problems.

## 1. Introduction

In engineering practice, the factor of safety (FoS) describes a relation between the applied loads and the load capacity of the system. The FoS is ubiquitously used for static and seismic design [1–5]. Foundation design requires a secure system that has a larger static resistive capacity than the applied loads to avoid bearing capacity failure. For seismic foundation design, a more complex and nuanced dynamic analysis is needed to understand if short-duration transient loads exceed capacity without significant damage to the overall system.

For the shallow foundations, a minimum vertical factor of safety ($FS_v$) (i.e., the ratio of the bearing capacity of the shallow foundation to the vertically applied load) of 3.0 is commonly used to avoid the bearing capacity failure due to uncertainty in the magnitudes of the loads and the soil parameters [4,6,7]. For seismic design for the foundations, most design codes seek to avoid the full mobilization of the bearing capacity of the foundation during earthquakes. These code provisions require the system to exhibit the elastic-linear behavior for the soil-foundation system [4,8–11]. Hence, sliding and rocking (uplift) responses of the foundation are prohibited in the codes. This results in a more conservatively-designed foundation that would have larger $FS_v$ than the recommended minimum value of 3.0.

For rocking shallow foundation, $FS_v$ is a crucial design parameter that determines seismic performance of the foundation-structure system [12–16]. Foundation-rocking behavior effectively reduces the structural seismic loads [17,18]. The rocking effect of the foundation, on the other hand, causes permanent deformation in the soil by mobilizing the nonlinear characteristics of the soil during earthquakes [19–22]. A balanced and well-designed system of rocking in the shallow foundation limits the structural seismic response and the foundation deformation, simultaneously [23]. Note that the $FS_v$ for the shallow foundation is estimated by the relation between the bearing capacity and the vertically applied loads from the superstructure and foundation.

Although systems with an identical bearing capacity of the foundation and applied load (i.e., an identical $FS_v$), the distribution of the combined applied load of the foundation and structure can vary from heavy foundations and light structures–to–lighter foundations and heavy structures. The parameter $FS_v$ treats these different inertial-systems as having similar load/capacity properties, although clearly the dynamic responses for the structure and foundation would be different owing to differing ratios of the inertial loads contributed by the structure and the foundation.

Dynamic soil-foundation-structure interaction (SFSI) links the soil-foundation system response to the foundation-structural response. The SFSI effect identifies the effects of different structure-to-foundation mass ratio ($MR$) (i.e., superstructural mass divided by foundation mass) on the

* Corresponding author.
*E-mail addresses:* kwko@berkeley.edu (K.-W. Ko), rkayen@berkeley.edu (R.E. Kayen).

https://doi.org/10.1016/j.soildyn.2023.108050
Received 9 February 2022; Received in revised form 16 February 2023; Accepted 18 May 2023
Available online 25 May 2023

overall system response [24–26]. Safak [24] investigated the transfer functions of structures and foundations depending on the *MR* using a two-degree-of-freedom (2DOF) analytical model with structural horizontal response and foundation swaying motion. Safak [24] discovered that the SFSI effect became significant as the *MR* value increased. However, the 2DOF analytical model from Safak [24] did not consider the nonlinearity of soil and the rocking of the foundation. Zhang and Tang [25] evaluated the SFSI effects of structures on shallow foundations that could sway and rock when subjected to ground motions. They noted SFSI effects were insensitive to *MR* for heavier structure and lighter foundation cases (*MR* from 1 to 10).

The SFSI inertial interaction is associated with the structural inertial behavior which in turn leads to foundation swaying and rocking, and permanent soil-foundation deformation [27,28]. Period lengthening of the structure due to inertial interaction has been investigated using the time-frequency domain [29], and a suite of proposed dimensionless parameters, associated with the soil, foundation, and structural properties, such as soil-to-structure stiffness ratio, structure-to-soil mass ratio, structural aspect ratio, and structure-to-foundation mass ratio [25,27,30–32] have been useful for isolating and evaluating the effects of system properties on SFSI.

A well-developed analytical solution for the SFSI system can provide closed-form solutions and adequate dynamic responses with valuable insight into the physical mechanisms underlying SFSI effects [33–39]. A governing equation of the 3DOF SFSI system including structural horizontal, foundation swaying, and rocking responses was studied in the previous works [35–39].

The objective of this study is to extend the 3DOF analytical model to include non-linear soil-foundation behavior and investigate the effect of the structure-to-foundation mass ratio on the SFSI effect during earthquakes. Here, the effect of *MR* on SFSI behavior is investigated from various perspectives. First, the SFSI dimensionless parameters excluding *MR* and $FS_v$ are fixed for a parametric study. The SFSI analytical model and methodologies to reflect the nonlinearity of soil into foundation stiffnesses and damping are developed, and the solution form is validated through centrifuge test results. The acceleration time histories and time-frequency domains for the structure, foundation swaying, and rocking responses are explored. The foundation-structural responses are correlated to each other by analysis of coherence and phase angle differences between the input motion and foundation response, and between the foundation and structural response depending on *MR* and $FS_v$.

## 2. SFSI analytical model and methodology for solving the model

### 2.1. 3DOF SFSI model

In this study, a dynamic system of the structure-foundation during earthquakes is expressed as the 3DOF SFSI model with structural net ($u_{net}$), foundation swaying ($u_{rf}$), and rocking ($u_\theta$) responses (Fig. 1). In the previous literature, a simplified SFSI model with a single-degree-of-freedom (SDOF) structure excluding the mass and the moment of inertia of the foundation has been used to focus on the inertial interaction effect of the structure [27,40]. A 3DOF SFSI model allows the foundation to fully and more freely interact with the soil and the superstructure during earthquakes. The equation of dynamic motion of the 3DOF model was derived using Lagrange's equation [41] and is presented in Eq. (1) [18,35–37,42].

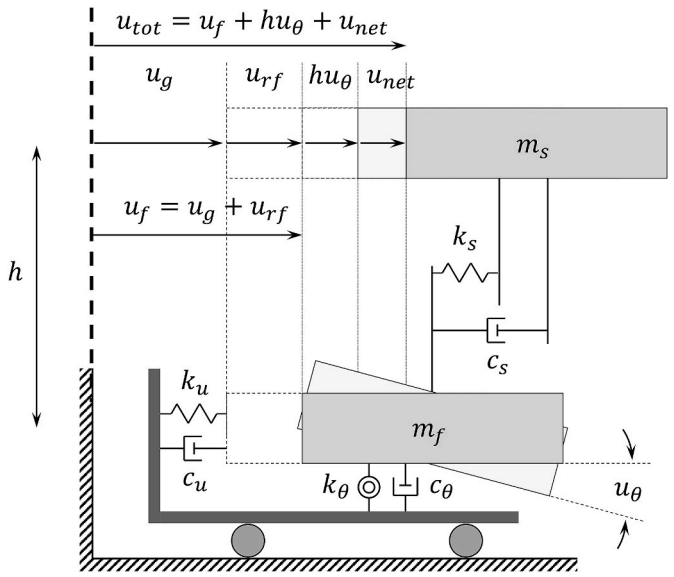


**Fig. 1.** 3DOF soil-foundation-structure system with structural net ($u_{net}$), foundation swaying ($u_{rf}$), and foundation rocking ($u_\theta$) responses.

where $m_s$ and $m_f$ are the mass of the structure and foundation, respectively; $I_f$ is the moment of inertia of the foundation; $h$ is the structural height; $c_s$, $c_u$, and $c_\theta$ are the structural damping and the damping of the foundation for swaying and rocking motions, respectively; $k_s$, $k_u$, and $k_\theta$ are the structural effective stiffness and the stiffnesses for the foundation for swaying and rocking motions, respectively; and $\ddot{u}_g$ is the acceleration of the input motion. The parameter $u_{net}$ measures the structural horizontal net response due to its flexibility. Parameter $u_{rf}$ is the foundation swaying motion relative to the input motion (free-field motion of the soil). $u_f$ is the foundation horizontal response, summation of $u_{rf}$ and $u_g$, and $u_{tot}$ is the total response of the structural horizontal motion including $u_{net}$, $u_f$, and $hu_\theta$ which the foundation rocking contributes to the structural horizontal response. The first, second, and third rows of Eq. (1) describe the horizontal structural, foundation swaying, and foundation rocking motions, respectively. The governing equation, Eq. (1), assumes the decoupled foundation swaying and rocking motions.

The soil-foundation interface regarding the foundation swaying and rocking motions expresses the foundation stiffness and damping for each of the motions in the 3DOF model. The stiffnesses of the embedded foundation are expressed, as below [27,28]:

$$k_u = \frac{8}{2-\nu} G r_u \times \left(1 + \frac{2}{3}\frac{e}{r_u}\right) \tag{2}$$

$$k_\theta = \frac{8}{3(1-\nu)} G r_\theta^3 \times \left(1 + 2\frac{e}{r_\theta}\right) \tag{3}$$

where $\nu$ is Poisson's ratio of soil; $G = \rho V_s^2$, $\rho$, and $V_s$ are the shear modulus, density, and the shear wave velocity of soil, respectively; $e$ is embedment depth of soil; and $r_u$ and $r_\theta$ are effective foundation radii for swaying and rocking motions, respectively. The $k_u$ and $k_\theta$ correspond to the elastic stiffnesses when the maximum shear modulus ($G_{max}$) applies

$$\begin{bmatrix} m_s & m_s & m_s h \\ m_s & m_s + m_f & m_s h \\ m_s h & m_s h & m_s h^2 + I_f \end{bmatrix} \begin{bmatrix} \ddot{u}_{net} \\ \ddot{u}_{rf} \\ \ddot{u}_\theta \end{bmatrix} + \begin{bmatrix} c_s & 0 & 0 \\ 0 & c_u & 0 \\ 0 & 0 & c_\theta \end{bmatrix} \begin{bmatrix} \dot{u}_{net} \\ \dot{u}_{rf} \\ \dot{u}_\theta \end{bmatrix} + \begin{bmatrix} k_s & 0 & 0 \\ 0 & k_u & 0 \\ 0 & 0 & k_\theta \end{bmatrix} \begin{bmatrix} u_{net} \\ u_{rf} \\ u_\theta \end{bmatrix} = - \begin{bmatrix} m_s \\ m_s + m_f \\ m_s h \end{bmatrix} \ddot{u}_g \tag{1}$$

to Eqs. (2) and (3). As $G$ for the foundation stiffness varies with the depth of the soil profile where the foundation is located, NEHRP [28] recommends the effective profile depth to estimate $G$ at the depth of $0.75\times r_u$ and $0.75 \times r_\theta$ for swaying and rocking motions, respectively. The $G$ at a depth of $0.75 \times r_u$ and $0.75 \times r_\theta$ minimizes the difference between the foundation stiffnesses on the elastic half-space and various non-uniform soil profiles [43]. FEMA 356 [44] introduces the effective shear modulus ratio ($G/G_{max}$) as a function of the peak ground acceleration (PGA) and average shear wave velocity of the site to reflect the nonlinearity of the soil into the foundation stiffness. However, $G/G_{max}$ for the foundation stiffness is not directly associated with the PGA of the soil but depends on the shear strain of the soil ($\gamma$). Accordingly, this study developed an SFSI analytical model that incorporated the nonlinearity of soil based on the shear strain. The following section will discuss how to apply $G/\ G_{max}$ depending on $\gamma$ and the foundation dynamic response to the foundation stiffnesses for solving the analytical model.

### 2.2. Step-by-step procedure to solve the governing equation of the 3DOF model

The SDOF structure was assumed as the linear-elastic structure to focus on the nonlinearity of the foundation behavior. The parameters relevant to the structure ($m_s$, $k_s$, $c_s$, and $h$) were given as fixed values at the beginning of solving Eq. (1). The dynamic responses of each of the modes ($u_{net}$, $u_{rf}$, and $u_\theta$) were computed through a step-by-step approach according to the time-step of the input motion. The procedure assumed that the soil followed the initial $G/G_{max}$ during an earthquake. The procedure includes the following steps.

1 Determine the input parameters corresponding to the targeted foundation-structure system. $k_u$ and $k_\theta$ should be the elastic stiffnesses by applying $G_{max}$ to Eqs. (2) and (3) at the initial time-step. This study inferred initial values of $c_u$ and $c_\theta$ from the curve of foundation damping ratio with $u_\theta$ (Fig. 2a).
2 Obtain the time history of the input motion which could be free-field soil surface affecting the foundation motion. The input motion should be a discrete signal having $n$ time-steps.
3 Solve the SFSI governing equation, Eq. (1), from the 1st time-step to the $i$ th time-step ($1 \le i \le n-1$). Velocity and displacement responses for three modes are zero at the 1st time-step as initial conditions.
4 Obtain the foundation responses at the $i$ th time-step. $u_{rf}(i)$ and $u_\theta(i)$ are the displacement response of the foundation swaying and the rotation of the foundation rocking, respectively.
5 Estimate the shear strain due to the foundation swaying, $\gamma_u(i)$, using $u_{rf}(i)$ and the effective profile depth for the swaying motion at the $i$ th time-step, as follows:

$$\gamma_u(i) = u_{rf}(i) \,/\, (0.75 \times r_u) \tag{4}$$

6 Estimate the shear modulus of soil and the stiffness and damping parameters regarding the foundation for the $(i+1)$ th time-step using the effective shear modulus ratio corresponding to $\gamma_u(i)$, $(G/G_{max})_{\gamma_u(i)}$, based on the shear modulus reduction curve (Fig. 2b) and the foundation damping ratio corresponding to $u_\theta(i)$, $\xi_\theta(i)$, based on the foundation damping curve (Fig. 2a), as below.

$$G(i+1) = (G/G_{max})_{\gamma_u(i)} \times G_{max} \tag{5}$$

$$k_u(i+1) = (G/G_{max})_{\gamma_u(i)} \times k_u \tag{6}$$

$$k_\theta(i+1) = (G/G_{max})_{\gamma_u(i)} \times k_\theta \tag{7}$$

$$c_u(i+1) = \xi_\theta(i) \times 2\sqrt{m_f k_u(i+1)} \tag{8}$$

$$c_\theta(i+1) = \xi_\theta(i) \times 2\sqrt{I_f k_\theta(i+1)} \tag{9}$$

7 Update the values of $G$, $k_u$, and $k_\theta$ by $G(i+1)$, $k_u(i+1)$, and $k_\theta(i+1)$ only if $G(i+1)$ is less than the previous minimum value of $G$. Update the values of $c_u$ and $c_\theta$ by $c_u(i+1)$ and $c_\theta(i+1)$ only if $\xi_\theta(i+1)$ exceeds the previous maximum value of $\xi_\theta$. Otherwise, the values of $G$, $k_u$, $k_\theta$, $c_u$, and $c_\theta$ are not updated.
8 Solve Eq. (1) for the next time-step, $i+1$, with the foundation stiffnesses and damping coefficients from step 7
9 Iterate steps 4 to 8 until $i+1 = n$.

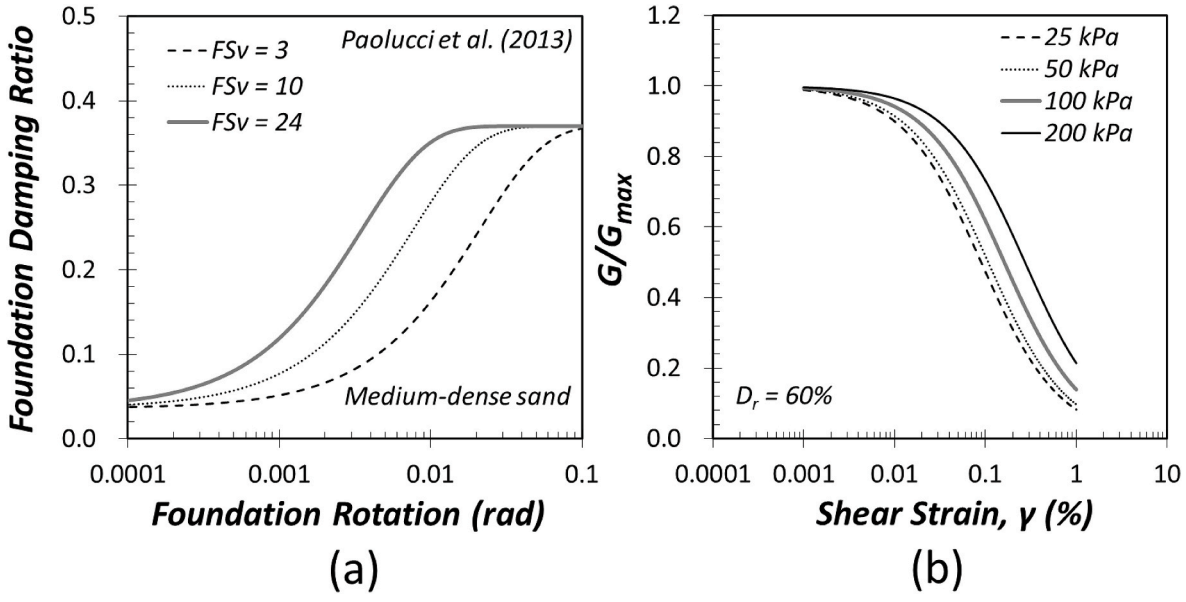


**Fig. 2.** Experimental curves for solving the analytical governing equation: (a) foundation damping ratio with foundation rotation angle of medium-dense sand from Paolucci et al. [45]; and (b) shear modulus reduction curves with confining stress for Silica sand with 60% of relative density.

## 3. Test parameters for analytical model

The following SFSI parameters were held fixed for the parametric studies of $FS_v$ and *MR:* soil-to-structure stiffness ratio, structural aspect ratio, $V_s$ profile of the soil site, and dimensions of the foundation and the structure such as the foundation length ($L$), $e$, and $h$. Only $m_s$ and $m_f$ were allowed to vary according to the $FS_v$ and *MR*.

### 3.1. Factor of safety, $FS_v$

The $FS_v$ is associated with the ultimate moment capacity of the shallow foundation and minimum contact area between the soil and foundation that resists the applied vertical load during foundation uplift [14,17,46]. The ultimate moment capacity of the foundation limits the structural seismic loads, and is called the rocking effect [18], such that $FS_v$ is strongly connected with the seismic responses of the foundation-structure system. Gajan and Kutter [23] recommended an optimized system for a rocking shallow foundation system with $FS_v = 10$ that does not suffer significant permanent deformation but effectively dissipates seismic energy. Here, the design $FS_v$ exceeds the minimum required value of $FS_v = 3.0$ to satisfy the seismic design guidelines limiting the non-linear behavior of the foundation. Public Works Research Institute (PWRI) in Japan corroborated the $FS_v$ of the constructed shallow foundations for high bridges and reported the $FS_v$ of the foundations was in the range of 9–24 [6,47]. In this study, the parameters for $FS_v$ were determined for 3, 10, and 24 to reflect the broad range from design code – to the recommendation of Gajan and Kutter [23] – to the PWRI upper bound $FS_v$. With the foundation dimensions and soil properties set at fixed values, the change of $FS_v$ directly reflects the change of applied vertical load equal to $(m_s + m_f) \times g$, where $g$ is gravitational acceleration.

### 3.2. Structure-to-foundation mass ratio, MR

For a given $FS_v$, the distribution of the applied vertical load for the system can be adjusted through the *MR* ($m_s/m_f$). Zhang and Tang [25] mentioned the practical range of *MR* ($m_s/m_f$) of 1–10, and the experimental database of rocking shallow foundation [48] showed the range of *MR* from 2 to 18. For this study, the *MR* was set as 2, 10, and 18 to cover this range. The range indicates that the structure mass is typically heavier, or much heavier, than the foundation mass. The lower *MR* is, the more dominant the inertia behavior of the foundation becomes. The parameter $k_s$ was varied in the study to preserve a constant structural natural period ($T_s$) since $T_s$ is a function of $m_s$ and $k_s$.

### 3.3. Physical properties of soil and 3DOF system

The physical properties of the soil-foundation-structure system for this study were based on the centrifuge models from Ko et al. [32]. The soil properties of the Silica sand used for the centrifuge tests were summarized in Table 1. As shown in Fig. 2b, the $G/G_{max}$ curves corresponding to 60% of the relative density of soil ($D_r$) was adopted from the resonant column test results for the Silica sand to reflect the nonlinearity of soil to the analytical solution. The foundation damping ratio curves for the medium-dense sand, a function of the $FS_v$ and $u_\theta$ were obtained from Paolucci et al. [45] (Fig. 2a). The dimensions of the foundation were assumed as $2 \times 2 \times 0.6$ m$^3$ (length $\times$ width $\times$ height), and the foundation model was fully embedded in the soil. The bearing capacity of the foundation was calculated by Meyerhof's equation [49] for the vertical bearing capacity of the shallow foundations and estimated to be 6877 kN.

**Table 1**
Silica soil model properties.

| Property | Value |
|---|---|
| Soil model properties | |
| Dry density, $\rho_d$ (t/m$^3$) | 1.46 |
| Relative density, $D_r$ (%) | 60 |
| Friction angle (°) | 39 |
| Shear wave velocity, $V_s$ (m/s) | 129 |

Nine foundation-structure models were evaluated in a test matrix controlled by the $FS_v$ and *MR*. Table 2 summarizes the models and their physical properties including the elastic structural, foundation swaying ($f_u$) and rocking ($f_\theta$) frequencies, not considering SFSI. Since the structural aspect ratio, structural height divided by foundation length ($h/L$), is one of the crucial dimensionless parameters for SFSI that determines the dominant behavior of the foundation-structure system between swaying and rocking [50], $h$ was fixed as 4.6 m corresponding to the structural aspect ratio of 2.3. Structural natural frequency ($f_s$) on the fixed-base condition was 2.5 Hz for all analytical models. Accordingly, structure-to-soil stiffness ($\sigma = V_s/f_s h$) was a constant value of 11.2.

The Hachinohe and Ofunato earthquake records from the $\boldsymbol{M}_w$7.9 Tokachi-Oki earthquake of May 16, 1968 and the $\boldsymbol{M}_w$7.4 Miyagi-Ken Oki earthquake of June 12, 1978 were used as the input motions to represent long period and short period dominated earthquake signals, respectively (Fig. 3). The two input motions have frequency energy corresponding to the structural natural frequency of 2.5 Hz, and the amplitudes of the PGA's were scaled to 0.16 g, 0.44 g, and 0.67 g to represent weak, moderate, and strong earthquakes. The amplitudes of the PGA's were decided based on the centrifuge tests from Ko et al. [32]. In total, three models of $FS_v$ and *MR*, subjected to two of input motions, each scaled to three PGA's gives the study fifty-four cases for the parametric analysis.

## 4. Comparison of analytical solutions with centrifuge test results

The analytical model and its methodology are compared with centrifuge results and validated through quality control studies, presented in Ko et al. [32]. The centrifugal acceleration was 20 g-level and silica sand with 60% of $D_r$ reconstituted the ground model with the height of 11.6 m on the prototype scale (Fig. 4a). Accelerometers were horizontally installed on the free-field soil surface, the foundation, and the structure, and the other two accelerometers were vertically attached to the foundation to measure the foundation rocking response. Physical properties of the validated centrifuge test model are tabulated in Table 3 and detailed information on the test can be found in Ref. [32].

The acceleration response of the free-field soil surface from the centrifuge test was used for the input motion ($\ddot{u}_g$) of the analytical models. Fig. 4b–c shows the foundation-structural dynamic responses of the centrifuge results and analytical solutions during a strong input (Hachinohe earthquake, input PGA: 0.80 g). In aspects of peak responses, the difference of $u_{net}$ and $u_{rf}$ between the centrifuge and the analytical model is only 7%, while the $u_\theta$ of the centrifuge model is larger than that of the analytical model by a factor of two. From 3 s to 8 s when most of the seismic energy is transferred from the input motion, the dynamic responses of the analytical model simulate reasonably well the phase information of the centrifuge model. After 8 s, $u_{net}$, $u_{rf}$, and $u_\theta$ of the analytical models have much longer periodic motion than the centrifuge results. The reduced shear modulus of the soil might recover after the end of the shaking in the centrifuge [51]. However, the shear modulus for the analytical model remains as it is reduced during the strong shaking motion, and it reveals, in turn, the longer period than the centrifuge responses. In displacement spectra, structural ($u_{net}$) and foundation swaying ($u_{rf}$) responses from the analytical model are consistent with that from the centrifuge test whereas foundation rocking ($u_\theta$) from the centrifuge test has a large amount of energy at 0.8 s than that from the analytical model. However, foundation-structural responses from the analytical and centrifuge results are generally comparable to each other in time and frequency domains.

**Table 2**
Properties of analytical models.

| Parameters | | | | | | | | | |
|---|---|---|---|---|---|---|---|---|---|
| Vertical factor of safety, $FS_v$ | 3 | 3 | 3 | 10 | 10 | 10 | 24 | 24 | 24 |
| Structure-to-foundation mass ratio, $MR$ ($m_s/m_f$) | 2 | 10 | 18 | 2 | 10 | 18 | 2 | 10 | 18 |
| Name of the model | FS3_MR2 | FS3_MR10 | FS3_MR18 | FS10_MR2 | FS10_MR10 | FS10_MR18 | FS24_MR2 | FS24_MR10 | FS24_MR18 |
| Structural mass, $m_s$ (kg) | 155950 | 212659 | 221613 | 46785 | 63797 | 66483 | 19493 | 26582 | 27701 |
| Foundation mass, $m_f$ (kg) | 77975 | 21265 | 12311 | 23392 | 6379 | 3693 | 9746 | 2658 | 1538 |
| Foundation moment of inertia, $I_f$ (kgm$^2$) | 35348 | 9640 | 5581 | 10604 | 2892 | 1674 | 4418 | 1205 | 697 |
| Structural height, $h$ (m) | 4.6 | 4.6 | 4.6 | 4.6 | 4.6 | 4.6 | 4.6 | 4.6 | 4.6 |
| Structural stiffness, $k_s$ (kN/m) | 38479 | 52471 | 54680 | 11543 | 15741 | 16404 | 4809 | 6558 | 6835 |
| Shear wave velocity of soil at the depth of $0.75 \times r_u$ | 256 | 256 | 256 | 189 | 189 | 189 | 155 | 155 | 155 |
| Static swaying stiffness of foundation, $k_u$ (kN/m) | 680091 | 680091 | 680091 | 370690 | 370690 | 370690 | 249316 | 249316 | 249316 |
| Static rocking stiffness of foundation, $k_\theta$ (kNm) | 1072752 | 1072752 | 1072752 | 584713 | 584713 | 584713 | 393263 | 393263 | 393263 |
| Structural natural frequency, $f_n$ (Hz) | 2.5 | 2.5 | 2.5 | 2.5 | 2.5 | 2.5 | 2.5 | 2.5 | 2.5 |
| Foundation swaying frequency, $f_u$ (Hz) | 14.9 | 28.5 | 37.4 | 20.0 | 38.4 | 50.4 | 25.5 | 48.7 | 64.1 |
| Foundation rocking frequency, $f_\theta$ (Hz) | 27.7 | 53.1 | 69.8 | 37.4 | 71.6 | 94.1 | 47.5 | 90.9 | 119.5 |

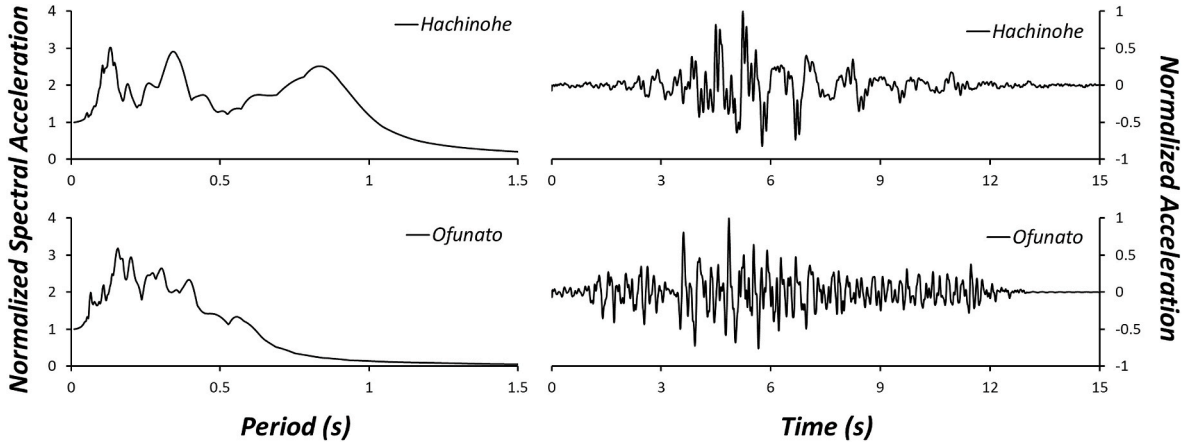


**Fig. 3.** Normalized acceleration response spectrum and acceleration time histories of input motions: Hachinohe and Ofunato earthquakes.

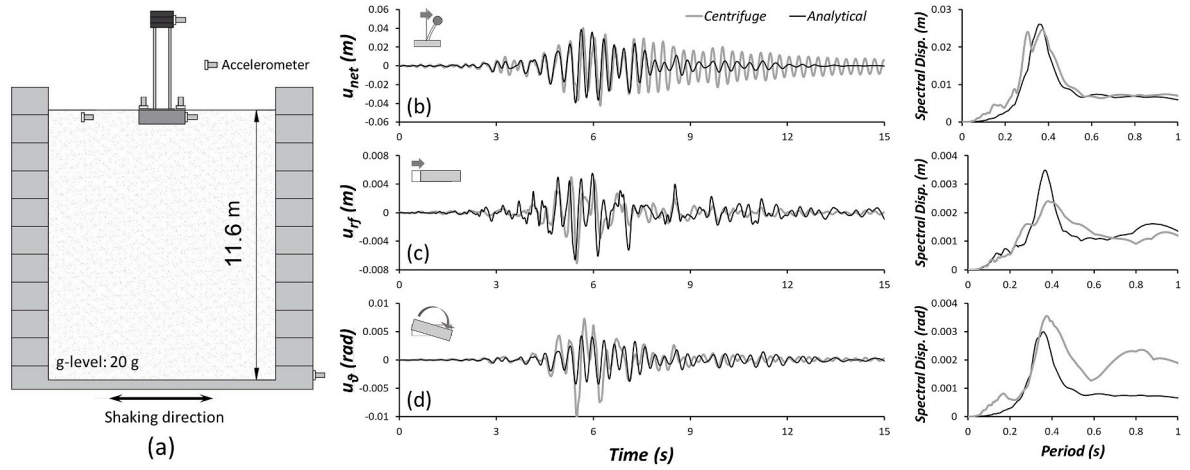


**Fig. 4.** Validated centrifuge test models and comparison of the foundation-structural dynamic responses between the analytical solution and centrifuge test results in time histories and displacement spectra: (a) cross-section of the dynamic centrifuge test model on prototype scale in shaking direction (modified from Ko et al. [32]); (b) structural net displacement; (c) foundation swaying displacement relative to the input motion; and (d) foundation rotation.

## 5. Analytical results and discussion

### 5.1. A representative result of analytical solution

A representative analytical solution of FS10_MR2 is presented in Fig. 5 for the strong condition of the Hachinohe input motion (PGA is 0.73 g). The soil-shear modulus reduction parameter $G/G_{max}$ gradually decreases to 70% at the initial stage of the input loading from 0 to 3 s, and then the soil significantly softens during the strong cycles (from 3 to 6 s) and soil shear stiffness reduces to less than 10% of $G_{max}$. Dynamic responses of the swaying and rocking modes follow the trend of $G/G_{max}$ reduction. The structural net response governs the system behavior at

**Table 3**
Physical properties of the validated centrifuge model.

| Property | Value |
|---|---|
| Shear wave velocity of soil, $V_s$ (m/s) | 85 |
| Structural mass, $m_s$ (kg) | 2216 |
| Structural stiffness, $k_s$ (kN/m) | 1210 |
| Structural damipng ratio (%) | 8 |
| Structural height, $h$ (m) | 3.6 |
| Foundation length, $L$ (m) | 2 |
| Foundation embedment, $e$ (m) | 0.6 |

the initial stage, whereas, when the amplitudes of the foundation responses ($u_{rf}$ and $u_\theta$) become more pronounced when the $G/G_{\max}$ decreases to 10%. The natural periods of $u_{net}$ and $u_\theta$ are visibly elongated after the reduction $G/G_{max}$. Interestingly, $u_\theta$ remains in phase with $u_{net}$. Conversely, $u_{rf}$ responds to the high-frequency components of the foundation swaying period.

### 5.2. Effects of MR on structural acceleration response

Seismic SFSI is not always beneficial for the structural response [52]. When the lengthened period of the structure is matched with the dominant energy of input motion, the SFSI effect is detrimental to the structural seismic response. The most intuitive approach to evaluate SFSI effects is to compare the structural seismic response considering SFSI with that on the fixed-base condition which neglects SFSI effects. The structural seismic acceleration response ($\ddot{u}_{fixed}$) on the fixed-base condition has been derived from Eq. (10).

$$m_s\ddot{u}_{fixed} + c\dot{u}_{fixed} + ku_{fixed} = -m_s\ddot{u}_g \tag{10}$$

The peak structural acceleration ratio ($\ddot{u}_{net}/\ddot{u}_{fixed}$) with the peak acceleration of input motion shows the SFSI effect on $FS_v$ and $MR$ (Fig. 6). For the conditions set in this study, the SFSI effects are entirely beneficial on the structural acceleration responses that are always less than the fixed case. The SFSI effects for these systems with $\sigma = 11.2$ show that the acceleration ratio decreases as the peak acceleration of the input motion increases. This indicates that the foundation responses govern the whole system behavior. SFSI effects thus show that as the acceleration ratio decreases the $FS_v$ decreases.

### 5.3. Acceleration time histories and time-frequency responses for the foundation-structure system

SFSI effects elongate not only the structural natural period but also the foundation natural periods because the reflection of the dynamic behaviors of the foundation increases the degree of freedom for the foundation-structure system. As the representative analytical solutions showed, the change of $G/G_{max}$ depends on the input motion, and the periods of the structure and foundation motions lengthen due to the nonlinearity of the soil-foundation-structure system.

The Stockwell transform is a useful method to observe the variation of the natural periods in the time-frequency domain over the time-

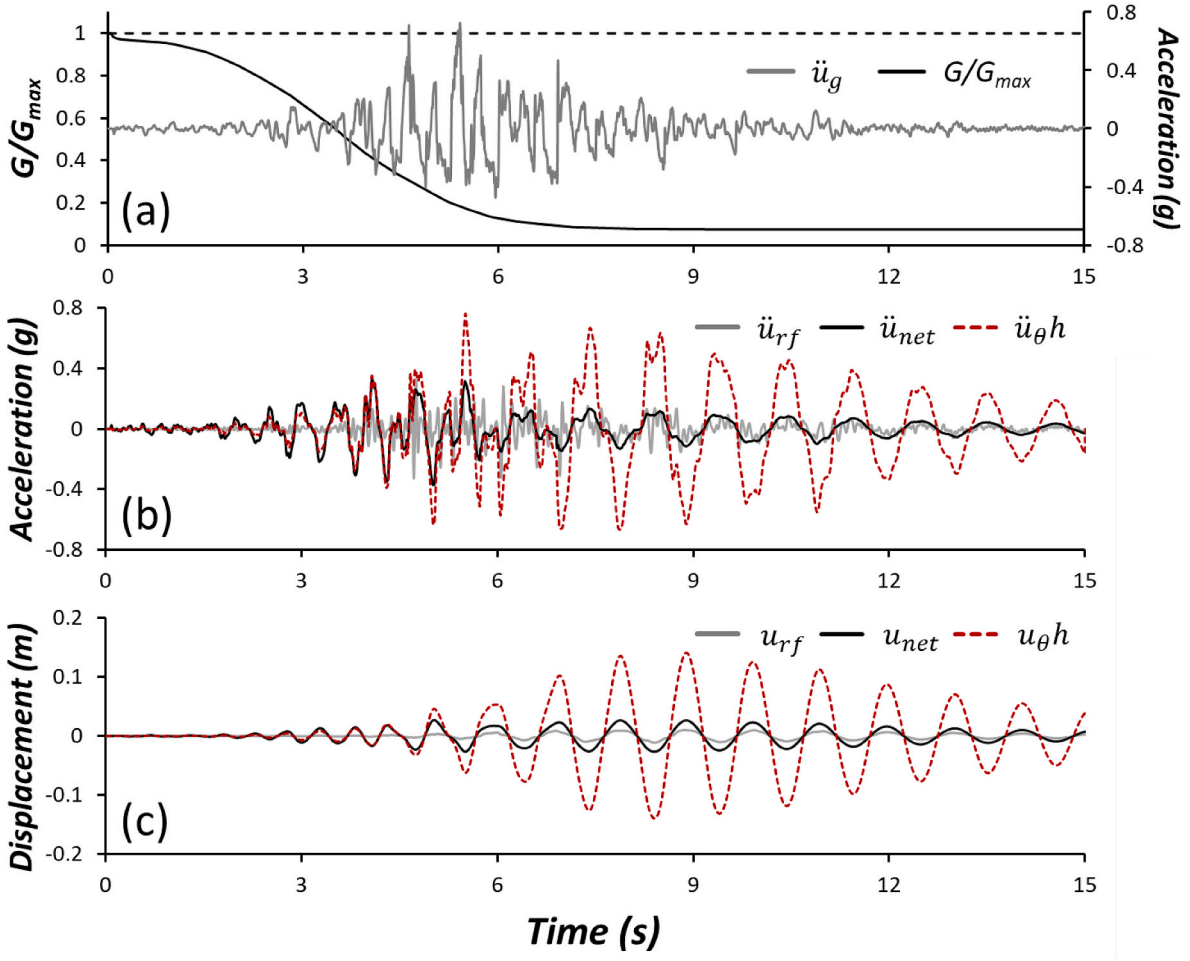


**Fig. 5.** A representative analytical solution of FS10_MR2 with Hachinohe input motion (PGA: 0.73 g): (a) acceleration time history of the input motion and $G/G_{max}$ reduction; (b) acceleration responses; and (c) displacement responses of the foundation swaying motion, structural net motion, and structural horizontal motion induced by foundation rocking.

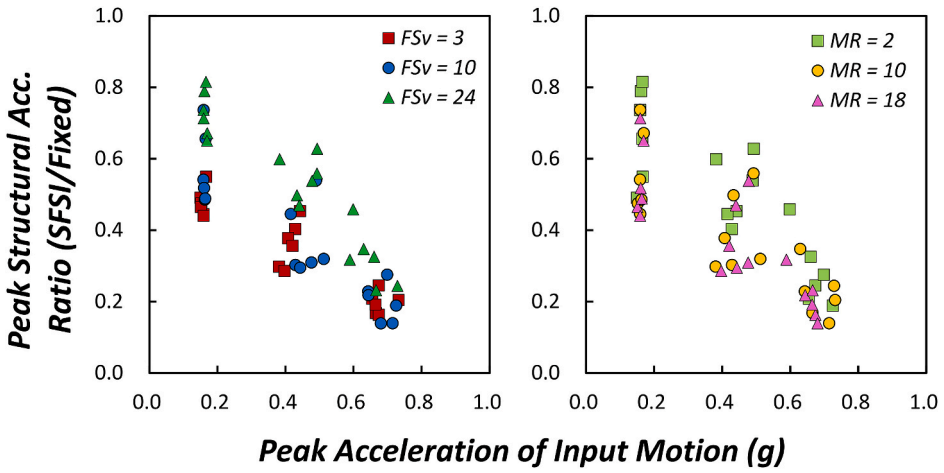


**Fig. 6.** Peak structural acceleration ratio with peak acceleration of input motion in aspects of $FS_v$ and *MR*.

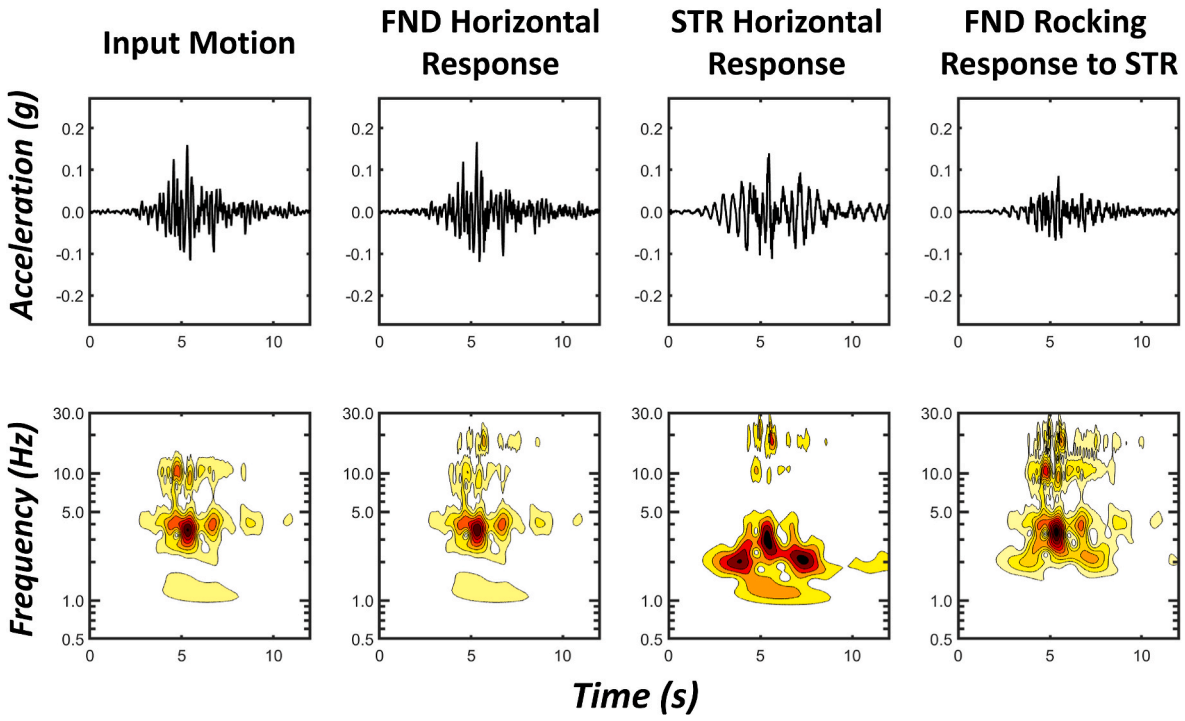


**Fig. 7.** Acceleration time histories and time-frequency responses for FS10_MR2 during the weak earthquake (Hachinohe, peak acceleration of input motion: 0.16 g).

history of earthquake shaking. In general, the foundation and structural responses were not different depending on the *MR* during weak earthquakes. Hence, for the weak earthquakes, Fig. 7 shows a representative acceleration time histories and time-frequency responses of $\ddot{u}_g$, $\ddot{u}_f$, $\ddot{u}_{tot}$, and $h\ddot{u}_\theta$. The foundation swaying motion generally follows the input motion and shows its natural frequency ($f_u$) closed to 20 Hz which is close to $f_u$ without considering SFSI. The structural motion includes large amounts of energy in its natural frequency close to 2.5 Hz and a small amount of energy corresponding to $f_u$ that reflects the structure also being affected by the foundation inertial motion. The foundation rocking motion shows smaller amplitudes than structure and foundation motions and it contains the frequency energies corresponding to the input earthquake motion, foundation swaying, and structural motions.

In contrast, during the strong earthquakes, the non-linearity was observed in the soil-foundation and the degree of softening depended on the *MR*. For the FS10_MR2 (the heavier foundation and the lighter structure case) during a strong earthquake (Fig. 8a), the foundation motion shows reduced natural frequencies in 10–20 Hz. Parameter $f_u$ gradually reduces with time owing to the nonlinearity of soil, and indicates that the heavier foundation inertial motion. The period lengthening combines both the structural and foundation motion. As expected, $f_s$ is reduced from 2.5 to a lower frequency around 1 Hz, is no longer affected by foundation and input motions. The foundation rocking motion follows the input motion at the initial stage (3–6 s), but is strongly governed by structural inertial motion rather than the input motion when the structural period has been significantly lengthened. Given the larger inertia of the heavier structure than the lighter structure, below, the period lengthening phenomenon is much clearer than for the lighter structure case (Fig. 8b). The $f_s$ significantly drops from 2.5 Hz to 0.6 Hz. For the lighter foundation and the heavier structure case, the foundation swaying motion follows the input motion, although the foundation rocking response follows the lighter foundation case.

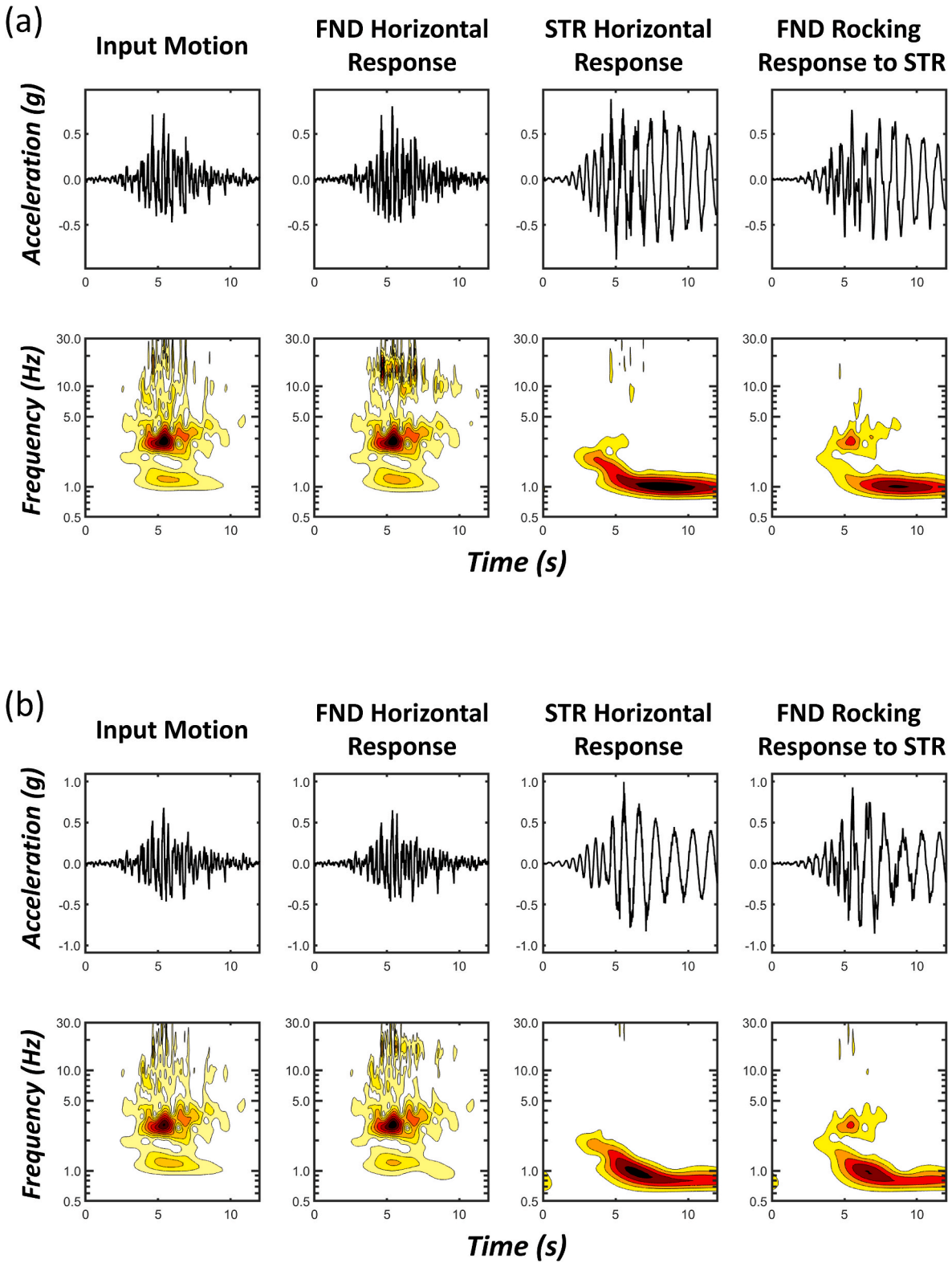


**Fig. 8.** Acceleration time histories and time-frequency responses during strong earthquakes: (a) FS10_MR2 (Hachinohe, peak acceleration of input motion: 0.73 g); and (b) FS10_MR18 (Hachinohe, peak acceleration of input motion: 0.68 g).

### *5.4. Effects of MR on coherence and phase angle difference between input motion, foundation response, and structural response*

Coherence and phase angle difference with frequency capture the independent dynamic responses of the foundation and structure (Fig. 9). That evaluation enables us to investigate which frequencies differ between the two motions. If the coherence is close to unity at a certain frequency, two motions are strongly correlated at that frequency. The heavier foundation (the lower *MR* case, FS3_MR2) manifests an independent dynamic behavior in response to the input motion (Fig. 9a). This is shown in the coherence between the input motion and foundation horizontal responses that decreases at 3–8 Hz and 16–21 Hz

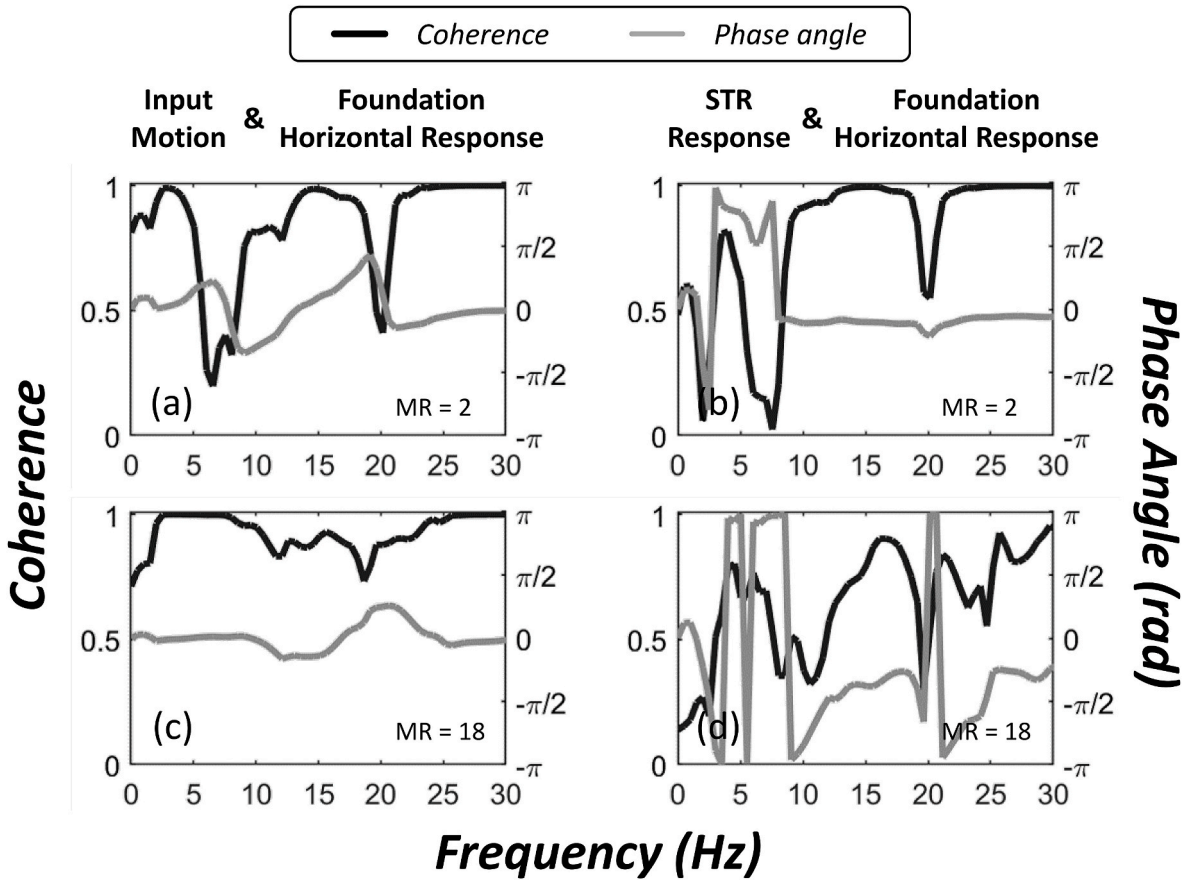


**Fig. 9.** Coherence and phase angle difference depending on *MR* during strong earthquakes (Hachinohe, peak acceleration of input motion: 0.66 g): (a) input motion and foundation horizontal response for FS3_MR2; (b) structural response and foundation horizontal response for FS3_MR2; (c) input motion and foundation horizontal response for FS3_MR18; and (d) structural response and foundation horizontal response for FS3_MR18.

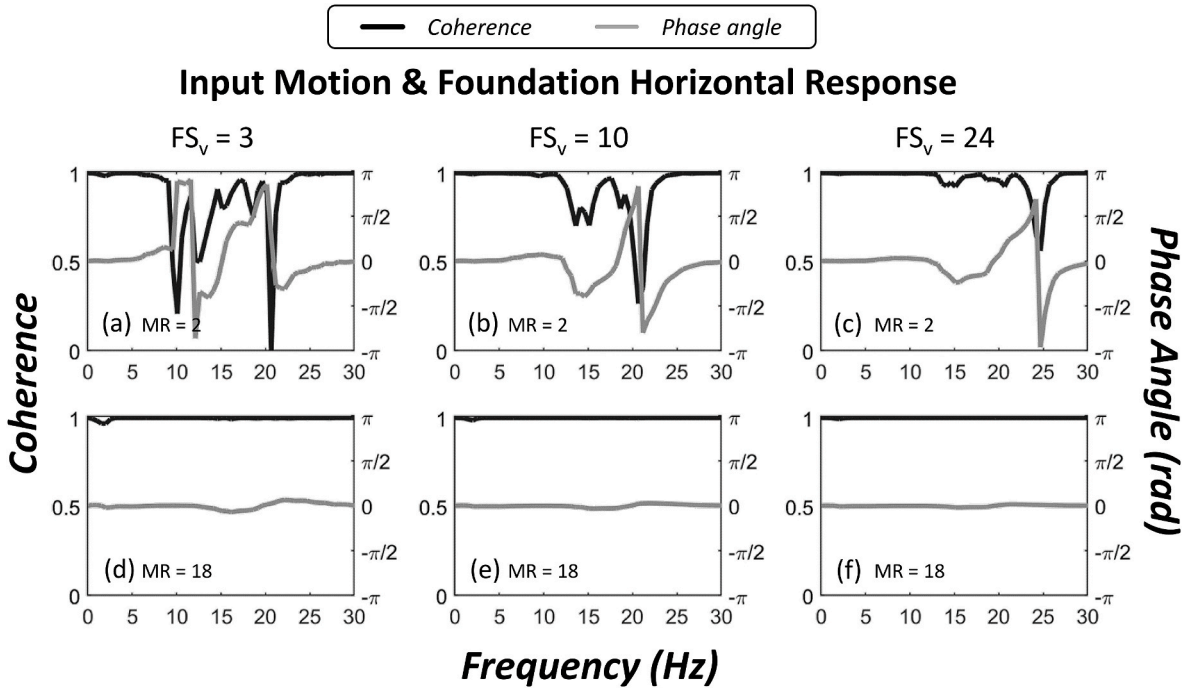


**Fig. 10.** Coherence and phase angle difference between input motion and foundation horizontal response depending on *MR* and $FS_v$ during weak earthquakes (Hachinohe, peak acceleration of input motion: 0.16 g): (a) FS3_MR2; (b) FS10_MR2; (c) FS24_MR2; (d) FS3_MR18; (e) FS10_MR18; and (f) FS24_MR18.

corresponding to the main energy of the input motion and $f_u$, respectively. At these frequencies, the phase angle difference also increases. Structural dynamic response barely correlates with foundation horizontal response at the reduced $f_s$, $f_u$, and the input motion (Fig. 9b). The frequencies components corresponding to the reduced $f_s$ and the input motions give rise to the phase difference between the structure and foundation responses rather than the $f_u$. On the other hand, the horizontal response of the lighter foundation (MR18) mostly follows the input motion (Fig. 9c). The heavier structure (FS3_MR18) exhibits an independent response from the foundation horizontal behavior due to its inertia.

The foundation inertial behavior for swaying motion also appears during earthquakes (Fig. 10). For example, heavier foundations (MR2) behave independently regardless of the input motions owing to its inertial motion while the lighter foundations (MR18) are strongly coupled with the input motions regardless of $FS_v$ during weak earthquakes. The inertial responses of the heavier foundations during weak earthquakes are also affected by their absolute mass. The coherence value between the foundation and input motions decreases and the phase angle difference becomes remarkable as the foundation mass gets larger despite the same *MR*. Moreover, massive foundations (FS3_MR2) have a reduction of $f_u$ relative to the lighter system (FS24_MR2) due to the difference of inertial behavior of the foundation attributed to the absolute value of the mass of the foundation.

### 5.5. Lengthened period of the structure and foundation swaying responses

Understanding the natural period of the foundation-structure system considering SFSI allows seismic design to avoid resonance effects. Although the input motions govern the foundation responses due to the kinematic interaction and this phenomenon could prevail for the embedded foundation, the foundation could suffer from resonance when elongated $f_u$ is matched with the main frequency energy of the input motion. The ratio of response spectrum (RRS) between the structure and input motions and that between the foundation swaying and input motions is used to derive the lengthened period of the structure and foundation. This RRS represents the transfer function of each system. It is the case that the system's natural periods increase with the peak acceleration of input motion due to the nonlinearity of the soil (Fig. 11). Since MR18 and MR2 systems manifest larger inertia from the structure and the foundation, respectively, each of the structure and foundation systems has elongated periods for the systems which correspond to have the larger inertia during earthquakes. The $f_u$ for MR2 at the static condition (Table 2) is much closer to the predominant seismic energy range of the input than that for MR10 and MR18 systems. Moreover, lengthened periods of the foundation swaying for MR2 are close to 0.1 s which corresponds to the predominant seismic energy range of the input motions. Accordingly, the peak acceleration of the foundation swaying responses is significantly larger for the foundations of MR2 systems due to resonance (Fig. 12). The peak acceleration of structural net responses, on the other hand, is less associated with the *MR*. It implies the permanent deformation of the system could be caused not by the structural inertial interaction effects but by the foundation inertial behavior for the heavier foundations.

## 6. Conclusions

This paper explored the effect of structure-to-foundation mass ratio on the dynamic responses of the SFSI system. To investigate the effects of structure-to-foundation mass ratio, other parameters effecting SFSI were fixed, and an analytical model and centrifuge validation methodology were introduced. The analytical model expressed the structural horizontal, foundation swaying, and rocking motions as a 3DOF SFSI model. The 3DOF analytical model was validated with the centrifuge test results. A parametric study was conducted using the fifty-four cases depending on *MR*, $FS_v$, input motions, and PGA intensity. The main findings of this study are summarized as follows:

1. SFSI effects of the cases for this study on the structural dynamic responses were evaluated by comparing the structural seismic responses considering SFSI with that on the fixed-base condition. SFSI effects of the cases were beneficial to the structural response with the effects most significant for cases where $FS_v$ decreased, and peak acceleration of the input motion.
2. The foundation horizontal and rocking responses were governed by the input motions during the weak earthquakes regardless of *MR*.
3. The heavier foundation manifested independent dynamic responses to the input motion during strong earthquakes by lengthened natural period. In contrast, the dynamic responses of the lighter foundation depended on the input motions during strong earthquakes. The foundation rocking response mostly followed the structural response in increased structural natural periods.
4. The heavier foundation developed its inertial behavior in response to the input motion regardless of the intensity of the input motions. The

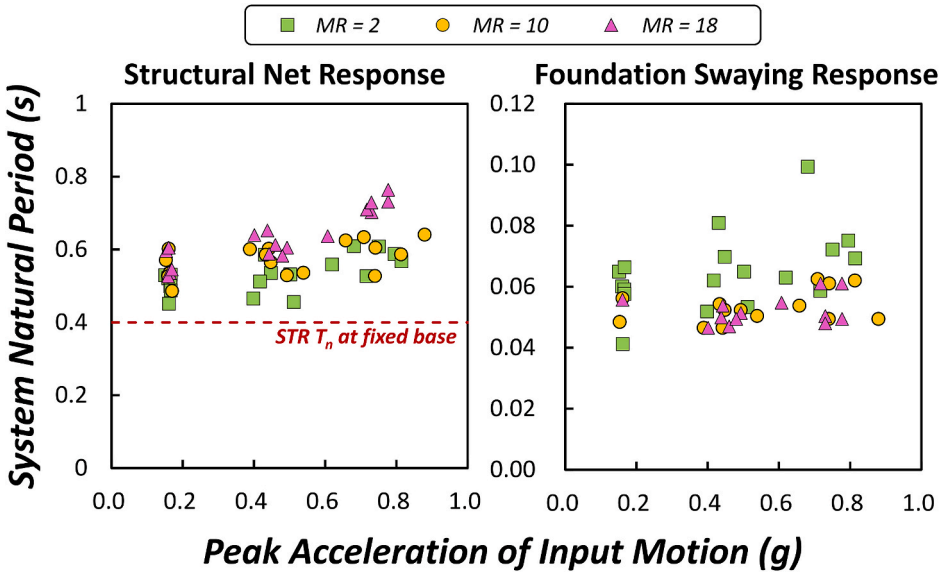


**Fig. 11.** Lengthened system natural period of the structure and the foundation swaying responses with peak acceleration of input motion.

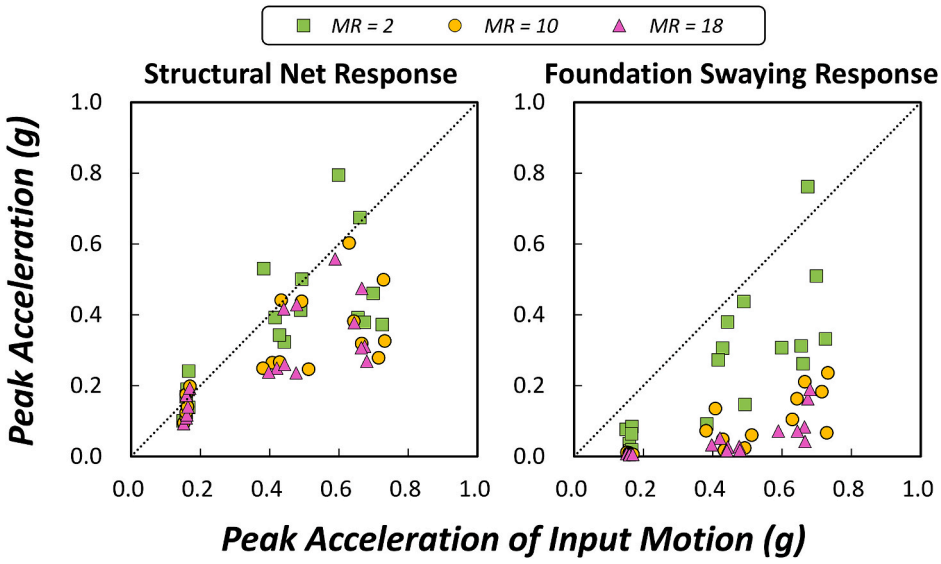


**Fig. 12.** Peak acceleration of the structural net and foundation swaying responses with peak acceleration of input motion.

phase differences of the foundation were mostly caused by the lengthened period of the foundation swaying motion. In the same vein, the heavier structure developed an inertial behavior independent of the input motion and foundation response.

5. As the structure-to-foundation mass ratio decreased, the natural period of the foundation swaying motion increased. Accordingly, a heavier foundation could suffer from the resonance when its lengthened period was matched with the input motion energy. Under that scenario, permanent deformation of the foundation-structure system would not be the result of the structural inertial, but by the foundation inertial response.

## Authors' statement

Kil-Wan Ko: Conceptualization, Methodology, Investigation, Data curation, Writing – Original Draft, Writing – Review & Editing, Robert Kayen: Methodology, Investigation, Writing – Review & Editing, Supervision.

## Declaration of competing interest

The authors declare that they have no known competing financial interests or personal relationships that could have appeared to influence the work reported in this paper.

## Data availability

Data will be made available on request.

## Acknowledgement

The authors would like to appreciate the late professor Dong-Soo Kim of KAIST, who gently guided the first author, Kil-Wan Ko, as a Ph.D. advisor. The Department of Civil and Environmental Engineering at the University of California, Berkeley is thanked for supporting Dr. Ko as a postdoctoral visiting researcher.

## NOMENCLATURE

| | |
|---|---|
| $c_s$ | Structural damping |
| $c_u$ | Damping coefficient of foundation swaying |
| $c_\theta$ | Damping coefficient of foundation rocking |
| $D_r$ | Relative density of soil |
| $e$ | Embedment depth of foundation |
| $FS_v$ | Vertical factor of safety for a shallow foundation |
| $f_s$ | Structural natural frequency |
| $f_u$ | Natural frequency of foundation swaying motion |
| $f_\theta$ | Natural frequency of foundation rocking motion |
| $G$ | Shear modulus of soil |
| $G_{max}$ | Maximum shear modulus of soil |
| $h$ | Height of structure |
| $I_f$ | Moment of inertia of foundation |
| $k_s$ | Stiffness for structure |
| $k_u$ | Swaying stiffness for foundation |
| $k_\theta$ | Rocking stiffness for foundation |
| $L$ | Foundation length |
| $MR$ | Structure to foundation mass ratio ($m_s/m_f$) |
| $m_s$ | Mass of structure |
| $m_f$ | Mass of foundation |

| | |
|---|---|
| $r_u$ | Effective foundation radius for swaying |
| $r_\theta$ | Effective foundation radius for rocking |
| $T_s$ | Structural natural period |
| $u_f$ | Foundation horizontal displacement |
| $u_{fixed}$ | Structural horizontal displacement on fixed base condition s |
| $u_g$ | Dynamic horizontal displacement of input motion |
| $u_{net}$ | Structural horizontal net displacement |
| $u_{rf}$ | Foundation horizontal displacement relative to input motion |
| $u_{tot}$ | Total displacement of the structural horizontal motion |
| $u_\theta$ | Rotation angle of foundation |
| $V_s$ | Shear wave velocity of soil |
| $\gamma$ | Shear strain of the soil |
| $\gamma_u$ | Shear strain due to foundation swaying response |
| $\nu$ | Poisson's ratio |
| $\rho$ | Density of soil |
| $\rho_d$ | Dry density of soil |
| $\xi_\theta$ | Damping ratio of foundation rocking |

## References


[1] Mononobe N, Matsuo H. On the determination of earth pressure during earthquake. Proc. World. Eng. Congr 1929;9:179–87.
[2] Okabe S. General theory on earth pressure and seismic stability of retaining walls and dams. J. Jpn. Civ. Eng. Soc. 1924;10(6):1277–323.
[3] Newmark NM. Effects of earthquakes on dams and embankments. Geotechnique 1965;15(2):139–59.
[4] Kimmerling RE, Bachus RC, Mayne PW, Scheider JA, Zettler TE. Geotechnical engineering circular no. 6, shallow foundations. Washington, DC: Federal Highway Administration; 2002.
[5] Gazetas G, Anastasopoulos I, Garini E. Geotechnical design with apparent seismic safety factors well-bellow 1. Soil Dynam Earthq Eng 2014;57:37–45.
[6] Shirato M, Kouno T, Asai R, Nakatani S, Fukui J, Paolucci R. Large-scale experiments on nonlinear behavior of shallow foundations subjected to strong earthquakes. Soils Found 2008;48(5):673–92.
[7] Cheney R, Chassie R. Soils and foundations workshop reference manual (No. FHWA NHI-00-045). Washington, DC: Federal Highway Administration; 2000.
[8] CEN. Eurocode 8: design of structures for earthquake resistance. Part 2: bridges. Final draft prEN 1998. Brussels: European Committee for Standardization; 2003.
[9] MOLIT. Guidelines for evaluating and improving earthquake resistance of existing facilities (foundation and ground). Korea: Ministry of Land, Infrastructure and Transport; 2020.
[10] Gazetas G. 4th Ishihara lecture: soil–foundation–structure systems beyond conventional seismic failure thresholds. Soil Dynam Earthq Eng 2015;68:23–39.
[11] Anastasopoulos I, Gazetas G, Loli M, Apostolou M, Gerolymos N. Soil failure can be used for seismic protection of structures. Bull Earthq Eng 2010;8:309–26.
[12] Anastasopoulos I, Kontoroupi T. Simplified approximate method for analysis of rocking systems accounting for soil inelasticity and foundation uplifting. Soil Dynam Earthq Eng 2014;56:28–43.
[13] Kokkali P, Abdoun T, Anastasopoulos I. Centrifuge modeling of rocking foundations on improved soil. J Geotech Geoenviron Eng 2015;141:04015041.
[14] Deng L, Kutter BL. Characterization of rocking shallow foundations using centrifuge model tests. Earthq Eng Struct Dynam 2012;41:1043–60.
[15] Gajan S, Kutter BL, Phalen JD, Hutchinson TC, Martin GR. Centrifuge modeling of load-deformation behavior of rocking shallow foundations. Soil Dynam Earthq Eng 2005;25:773–83.
[16] Ko KW, Ha JG, Park HJ, Kim DS. Soil-rounding effect on embedded rocking foundation via horizontal slow cyclic tests. J Geotech Geoenviron Eng 2018;144:04018004.
[17] Tsatsis A, Anastasopoulos I. Performance of rocking systems on shallow improved sand: shaking table testing. Front. Built Environ. 2015;1:9.
[18] Kim DK, Lee S, Kim D, Choo YW, Park H. Rocking effect of a mat foundation on the earthquake response of structures. J Geotech Geoenviron Eng 2015;141:04014085.
[19] Anastasopoulos I, Kourkoulis R, Gelagoti F, Papadopoulos E. Rocking response of SDOF systems on shallow improved sand: an experimental study. Soil Dynam Earthq Eng 2012;40:15–33.
[20] Deng L, Kutter BL, Kunnath SK. Centrifuge modeling of bridge systems designed for rocking foundations. J Geotech Geoenviron Eng 2012;138:335–44.
[21] Deng L, Kutter BL, Kunnath SK. Seismic design of rocking shallow foundations: displacement-based methodology. J Bridge Eng 2014;19:04014043.
[22] Ko KW, Ha JG, Park HJ, Kim DS. Centrifuge modeling of improved design for rocking foundation using short piles. J Geotech Geoenviron Eng 2019;145:04019031.
[23] Gajan S, Kutter BL. Capacity, settlement, and energy dissipation of shallow footings subjected to rocking. J Geotech Geoenviron Eng 2008;134:1129–41.
[24] Safak E. Detection and identification of soil-structure interaction in buildings from vibration recordings. J Struct Eng 1995;121:899–906.
[25] Zhang J, Tang Y. Dimensional analysis of structures with translating and rocking foundations under near-fault ground motions. Soil Dynam Earthq Eng 2009;29:1330–46.
[26] Ha JG, Ko KW, Jo SB, Park HJ, Kim DS. Investigation of seismic performances of unconnected pile foundations using dynamic centrifuge tests. Bull Earthq Eng 2019;17:2433–58.
[27] Stewart JP, Fenves GL, Seed RB. Seismic soil-structure interaction in buildings. I: analytical methods. J Geotech Geoenviron Eng 1999;125:26–37.
[28] NIST GCR 12-917-21. Soil-structure interaction for building structures. Gaithersburg: National Institute of Standards and Technology, US Department of Commerce; 2012.
[29] Pelekis I, Madabhushi GSP, DeJong MJ. Seismic performance of buildings with structural and foundation rocking in centrifuge testing. Earthq Eng Struct Dynam 2018;47:2390–409.
[30] Stewart JP. Variations between foundation-level and free-field earthquake ground motions. Earthq Spectra 2000;16:511–32.
[31] Veletsos AS, Meek JW. Dynamic behaviour of building-foundation systems. Earthq Eng Struct Dynam 1974;3:121–38.
[32] Ko KW, Ha JG, Park HJ, Kim DS. Investigation of period-lengthening ratio for single-degree-of-freedom structures using dynamic centrifuge test. J Earthq Eng 2021;25:1358–80.
[33] Mason HB, Trombetta NW, Chen Z, Bray JD, Hutchinson TC, Kutter BL. Seismic soil-foundation-structure interaction observed in geotechnical centrifuge experiments. Soil Dynam Earthq Eng 2013;48:162–74.
[34] Kayen R. Seismic displacement of gently-sloping coastal and marine sediment under multidirectional earthquake loading. Eng Geol 2017;227:84–92.
[35] Kim D, Hong-gun P, Kim D, Lee H. Nonlinear system identification on shallow foundation using Extended Kalman Filter, vol. 128; 2020.
[36] Tileylioglu S, Stewart JP, Nigbor RL. Dynamic stiffness and damping of a shallow foundation from forced vibration of a field test structure. J Geotech Geoenviron Eng 2011;137:344–53.
[37] Ko KW, Ha JG, Park HJ, Kim DS. Comparison between cyclic and dynamic rocking behavior for embedded shallow foundation using centrifuge tests. Bull Earthq Eng 2018;16:5171–93.
[38] Chandra J, Guéguen P. Nonlinear response of soil–structure systems using dynamic centrifuge experiments. J Earthq Eng 2019;23:1719–41.
[39] Xiong W, Jiang LZ, Li YZ. Influence of soil–structure interaction (structure-to-soil relative stiffness and mass ratio) on the fundamental period of buildings: experimental observation and analytical verification. Bull Earthq Eng 2016;14:139–60.
[40] Stewart JP, Fenves GL. System identification for evaluating soil-structure interaction effects in buildings from strong motion recordings. Earthq Eng Struct Dynam 1998;27:869–85.
[41] Craig JRR, Kurdila AJ. Fundamentals of structural dynamics. New Jersey: John Wiley & Sons, Inc; 2006.
[42] Ko KW, Ha JG, Kim DS. Analytical evaluation and experimental validation on dynamic rocking behavior for shallow foundation considering structural response. Earthq Eng Eng Vib 2022;21(1):37–51.
[43] Stewart JP, Kim S, Bielak J, Dobry R, Power MS. Revisions to soil-structure interaction procedures in NEHRP design provisions. Earthq Spectra 2003;19(3):677–96.
[44] FEMA. Prestandard and commentary for the seismic rehabilitation of buildings, FEMA 356. Washington, D.C.: Federal Emergency Management Agency; 2000.
[45] Paolucci R, Figini R, Petrini L. Introducing dynamic nonlinear soil-foundation-structure interaction effects in displacement-based seismic design. Earthq Spectra 2013;29:475–96.
[46] Gajan S, Kutter BL. Effect of critical contact area ratio on moment capacity of rocking shallow footings. J Geotech Geoenviron Eng 2008:1–11.

[47] Fukui J, Kimura Y, Ishida M, Kishi Y. An investigation on the response of shallow foundations to large earthquakes. Technical Memorandum of PWRI No. 3627. Tsukuba: Public Works Research Institute; 1999.
[48] Gavras AG, Kutter BL, Hakhamaneshi M, Gajan S, Tsatsis A, Sharma K, et al. Database of rocking shallow foundation performance: dynamic shaking. Earthq Spectra 2020;36:960–82.
[49] Meyerhof GG. Some recent Research on the bearing capacity of foundations. Can Geotech J 1963;1:16–26.
[50] Gajan S, Kutter BL. Effects of moment-to-shear ratio on combined cyclic load-displacement behavior of shallow foundations from centrifuge experiments. J Geotech Geoenviron Eng 2009;135:1044–55.
[51] Olga P, Kojiro I. Changes in shear moduli of liquefied and nonliquefied soils during the 1995 kobe earthquake and its aftershocks at three vertical-array sites. Bull Seismol Soc Am 2002;92(5):1952–69.
[52] Mylonakis G, Gazetas G. Seismic soil-structure interaction: beneficial or detrimental? J Earthq Eng 2000;4:277–301.